ELSEVIER

Journal of Nuclear Materials 253 (1998) 78–86

journal of nuclear materials

X-ray diffractometry and high-resolution electron microscopy of neutron-irradiated SiC to a fluence of 1.9×10^{27} n/m^2

T. Yano [a,*], H. Miyazaki [b], M. Akiyoshi [a], T. Iseki [b]

[a] *Research Laboratory for Nuclear Reactors, Tokyo Institute of Technology, 2-12-1, O-okayama, Meguro-ku, Tokyo 152, Japan*
[b] *Department of Inorganic Materials, Tokyo Institute of Technology, 2-12-1, O-okayama, Meguro-ku, Tokyo 152, Japan*

Abstract

Neutron-induced damage in SiC up to a fluence of 1.9×10^{27} n/m^2 ($E > 0.1$ MeV) was examined by means of X-ray diffractometry and high-resolution electron microscopy. Specimens of β-SiC were irradiated in fast breeder reactors at 370 to 650°C. The lattice parameters of all specimens were increased by the irradiation, but above 2×10^{26} n/m^2 lattice expansion decreased and was accompanied by significant peak broadening. Electron microscopy revealed a high density of interstitial loops on {111}, where X-ray diffraction peaks showed marked broadening. Peak broadening could be attributed mainly to the crystallite size effect at lower fluences, but a strain contribution was significant above 2×10^{26} n/m^2. Electron diffraction patterns and high-resolution images indicated preservation of crystallinity up to the highest fluence observed. Thermal annealing up to 1000°C did not affect the peak broadening and average loop diameter. Above 1400°C, decrease in lattice strain and increase in crystallite size with increasing annealing temperature were observed. © 1998 Elsevier Science B.V.

1. Introduction

The use of low-activation structural components, in particular continuous SiC fiber-reinforced SiC composite (SiC/SiC_f), for fusion power reactors is essential in terms of safety. Silicon carbide has numerous desirable properties, including low activation, rapid decay of activity, low atomic number, good thermal conductivity, excellent high-temperature properties, and corrosion resistance [1–6]. Furthermore, SiC shows good resistance to high energy neutron irradiation up to high doses [7–11]. If a SiC/SiC_f composite is used in the first-wall region of a fusion reactor, it will suffer from serious irradiation-induced damage by high energy neutrons. Even though much research has already been reported on neutron irradiation effects in SiC, it is still important to clarify neutron-induced changes, particularly those due to high dose irradiation.

It is generally accepted that SiC undergoes an isotropic expansion at irradiation temperatures below 1000°C. At about 3×10^{24} n/m^2, the expansion saturates at a level which depends strongly on irradiation temperature. The saturated level of the swelling decreases with increased irradiation temperature up to around 1000°C. The lattice parameter increase corresponds well with the increase in macroscopic dimension. Lattice and macroscopic length expansion originate mainly from point and point-like defects. Above 1200°C, expansion of macroscopic length increases due to formation of voids [12].

It was first reported by Price [13] that X-ray line broadening occurred in β-SiC irradiated to 5×10^{25} n/m^2 and that the degree of broadening increased after irradiation to 1×10^{26} n/m^2 [9]. We showed previously that the lattice parameter growth became smaller than the macroscopic length growth for fluences of 4.8×10^{26} and 1.7×10^{27} n/m^2, and significant broadening of X-ray diffraction peaks was observed [14]. From precise analysis of X-ray peak profiles, it was clarified that the broadening could be attributed mainly to the crystallite size effect at a fluence below 1.5×10^{26} n/m^2, but that a strain contribu-

* Corresponding author. Tel.: +81-3 5734 3380; fax: +81-3 5734 2959; e-mail: tyano@nr.titech.ac.jp.

PII S0022-3115(97)00331-0

tion was significant above 3.2×10^{26} n/m^2 [15]. It has also been reported that interstitial dislocation loops form on {111} in β-SiC irradiated to 4.8×10^{26} and 1×10^{27} n/m^2 [16,17].

In this study, further detailed examination of neutron fluence effects on damage creation in SiC is carried out by means of X-ray diffractometry coupled with a high-resolution electron microscopy. The effect of annealing on X-ray line broadening is also examined to clarify the irradiation response of SiC after high dose irradiation.

2. Experimental procedure

Small rods of β-SiC were fabricated by a reaction sintering method using semiconductor-grade Si and spectroscopically-pure C. After sintering, excess C and Si were removed by heating specimens at 800°C in air and at 1800°C in vacuum. The bulk density of the rods was about 85% of the theoretical value. Only the β (cubic) form of SiC was detected by X-ray powder diffraction analysis. The average particle size was about 3 μm. The specimens were neutron irradiated in fast breeder reactors at 370–650°C to fluences of 3.0×10^{24} to 1.9×10^{27} n/m^2 ($E >$ 0.1 MeV). The irradiation conditions are shown in Table 1. A portion of each specimen was thermally annealed at 750, 1000 and 1400°C under vacuum for 1 h before crushing.

X-ray powder diffraction analysis was carried out with a Philips PW-1700 diffractometer using Cu Kα radiation and a graphite monochrometer, and the profiles of peaks with indices (111), (220), (311), (331), (422) and (333)/(511) were obtained. For X-ray measurements, the material was carefully crushed into powder using a mortar. Instrumental broadening was calibrated using an unirradiated specimen. Corrected diffraction profiles were obtained by deconvolution of profiles from the irradiated and unirradiated specimens using the Stoke's method. The individual contributions of strain and crystallite size effects to broadening were calculated by the Warren–Averbach method [18]. The detailed procedures have been described elsewhere [15]. Lattice parameters were also obtained using Si as an internal standard ($a_0 = 0.534088$ nm).

A part of each specimen was sliced for electron microscopy before crushing. Thin foils were prepared by standard dimpling and ion-milling techniques. The transmission electron microscopes used in the present study were JEOL 200CX and Hitachi H-9000 instruments with accelerating voltages of 200 and 300 kV, respectively.

3. Results and discussion

3.1. Effect of fluence

The change in lattice parameter due to neutron irradiation is shown in Fig. 1. As mentioned above, it is known that the saturation level of lattice growth or linear expansion of SiC irradiated to a fluence below 5×10^{25} n/m^2 depends on the irradiation temperature [9]. The relation between the amount of lattice growth or linear expansion S (%) and irradiation temperature T (°C) between 400 and 600°C was obtained for fast reactor-irradiated SiC by Palentine [19] and is described by the equation $S = 0.81842 - 7.6355 \times 10^{-4} T$. The expected values of lattice growth based on this equation for each specimen are shown in Fig. 1. It is clear that below 2.0×10^{26} n/m^2, the lattice growth almost corresponds with the expected values, whereas beyond this fluence the lattice growth is much smaller.

Table 1
Neutron irradiation conditions and lattice parameter of SiC specimens used in this study

Neutron fluence (n/m^2) ($E > 0.1$ MeV)	Irradiation temperature (°C)	Lattice parameter (nm)
0 (reference)	–	0.43599
3.0×10^{24}	470	0.43801
2.1×10^{25}	530	0.43818
1.0×10^{26}	470	(not obtained)
1.5×10^{26}	370	0.43794
2.0×10^{26}	600	0.43735
3.2×10^{26}	530	0.43685
4.8×10^{26}	620	0.43648
1.0×10^{27}	650	0.43659
1.7×10^{27}	480	0.43628
1.9×10^{27}	570	(not obtained)

Profiles of the (333)/(511) reflection for various specimens with different fluences are shown in Fig. 2 [14,15]. The scale of intensity is different for each spectrum, and these spectra were shifted to avoid overlapping. Compared

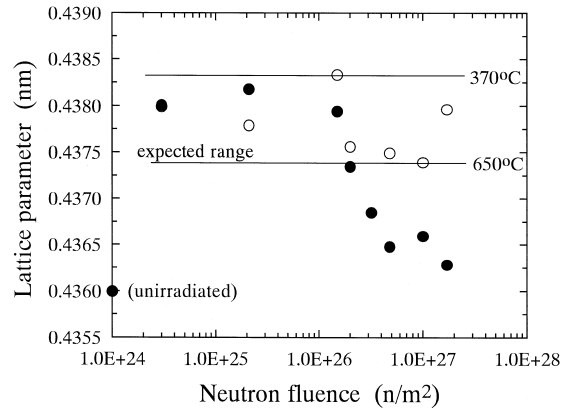

Fig. 1. Change in lattice parameter as a function of neutron fluence. Filled circles are measured values and open circles are calculated using the equation described by Palentine [19].

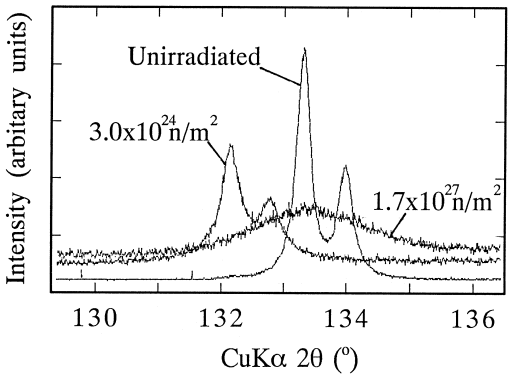

Fig. 2. X-ray diffraction profiles of the (333)/(511) reflection for unirradiated and irradiated SiC.

with the profiles from the unirradiated specimen, which consist of a pair of peaks corresponding $K\alpha_1$ and $K\alpha_2$ radiations, slight broadening occurred for a specimen irradiated to 3.0×10^{24} n/m^2. The reflection retained the double-peaks feature, but was shifted to a lower diffraction angle. This shift corresponds with expansion of the lattice spacing. On the other hand, appreciable broadening was present in the profile from the specimen irradiated to a fluence of 1.7×10^{27} n/m^2. There is no separation of $K\alpha_1$ and $K\alpha_2$ peaks. The fluence dependence of the full-width at half-maximum (FWHM) of the (333)/(511) reflection is shown in Fig. 3. Crystallite size and the root mean squared (rms) strain for each specimen were obtained by a Warren–Averbach analysis and are presented in Fig. 4. The FWHM of the (333)/(511) peaks may show a slight increase for the specimen irradiated to 1.5×10^{26} n/m^2 but markedly increases for specimens irradiated to 2.0×10^{26} n/m^2 or higher. The marked decrease of lattice growth and increase of peak FWHM happen concurrently in terms of irradiation fluence. Crystallite size gradually decreases up to a fluence of 1.5×10^{26} n/m^2, after which there is a sharp decrease. RMS strain sharply increases above a fluence of 3.0×10^{26} n/m^2.

Electron micrographs of specimens irradiated to 1.0×10^{26}, 4.8×10^{26}, 1.0×10^{27} and 1.9×10^{27} n/m^2 are shown in Fig. 5. Bright field images were taken along the ⟨110⟩ incident beam direction of β-SiC. In Fig. 5(a), only small features in dark contrast a few nm in diameter were observed. On the other hand, much larger features with straight line contrast at the center or edge of regions in dark contrast are visible in Fig. 5(b) to (d). The directions of the line contrast cross at an angle of 70°. Corresponding selected area diffraction patterns are inserted in the figure and indicate that the line contrast is parallel to {111}. The diffraction pattern in Fig. 5(a) shows no diffuse scattering. However, in Fig. 5(d), weak diffuse scattering along ⟨111⟩ is observed and is related to the dense faulted loop formation on {111}. Maximum diffuse scattering is due to a {111} twin in the crystal. In both cases, good crystallinity is indicated. Even at the highest fluence, the formation of voids was not detected.

High-resolution images of the same specimens in Fig. 5(a) and (c) are presented in Figs. 6 and 7, respectively. In Fig. 6, the lattice image of β-SiC is visible for the whole area without any detectable disturbance of lattice fringes. However, there are many patches of dark or bright contrast in the background with no apparent periodicity. These patches of contrast usually spread over about 10 to 20 dots. It is likely that these features correspond to small defects less than 1 nm in size. Defects in the periodic lattice larger than 1 nm should be visible by high-resolution electron microscopy. On the other hand, the change in stacking sequence along ⟨111⟩ is clearly observed in Fig. 7. Detailed analysis based on a multi-slice image simulation indicated that this defect is an interstitial-type dislocation loop with a thickness of one SiC layer [16]. In the case of the specimen irradiated to a fluence of 1.0×10^{27} n/m^2, the average loop diameter is about 15 nm and the number density is 5×10^{23}/m^3 [17]. The average defect size is

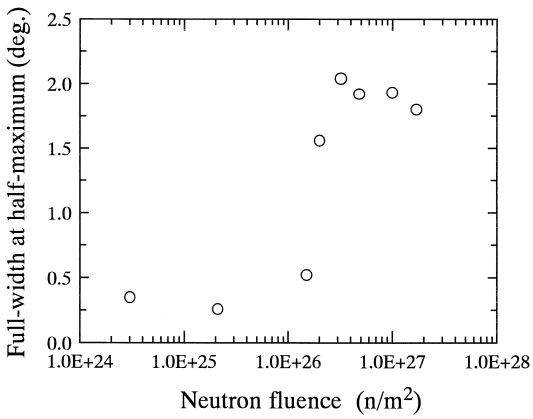

Fig. 3. Change in the full-width at half-maximum of the (333)/(511) reflection as a function of neutron fluence.

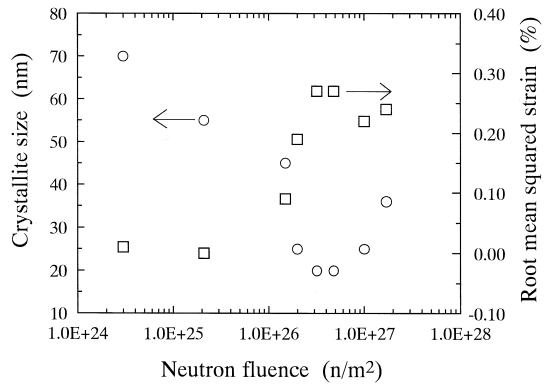

Fig. 4. Variations of crystallite size and the root mean squared strain of the specimens as a function of neutron fluence.

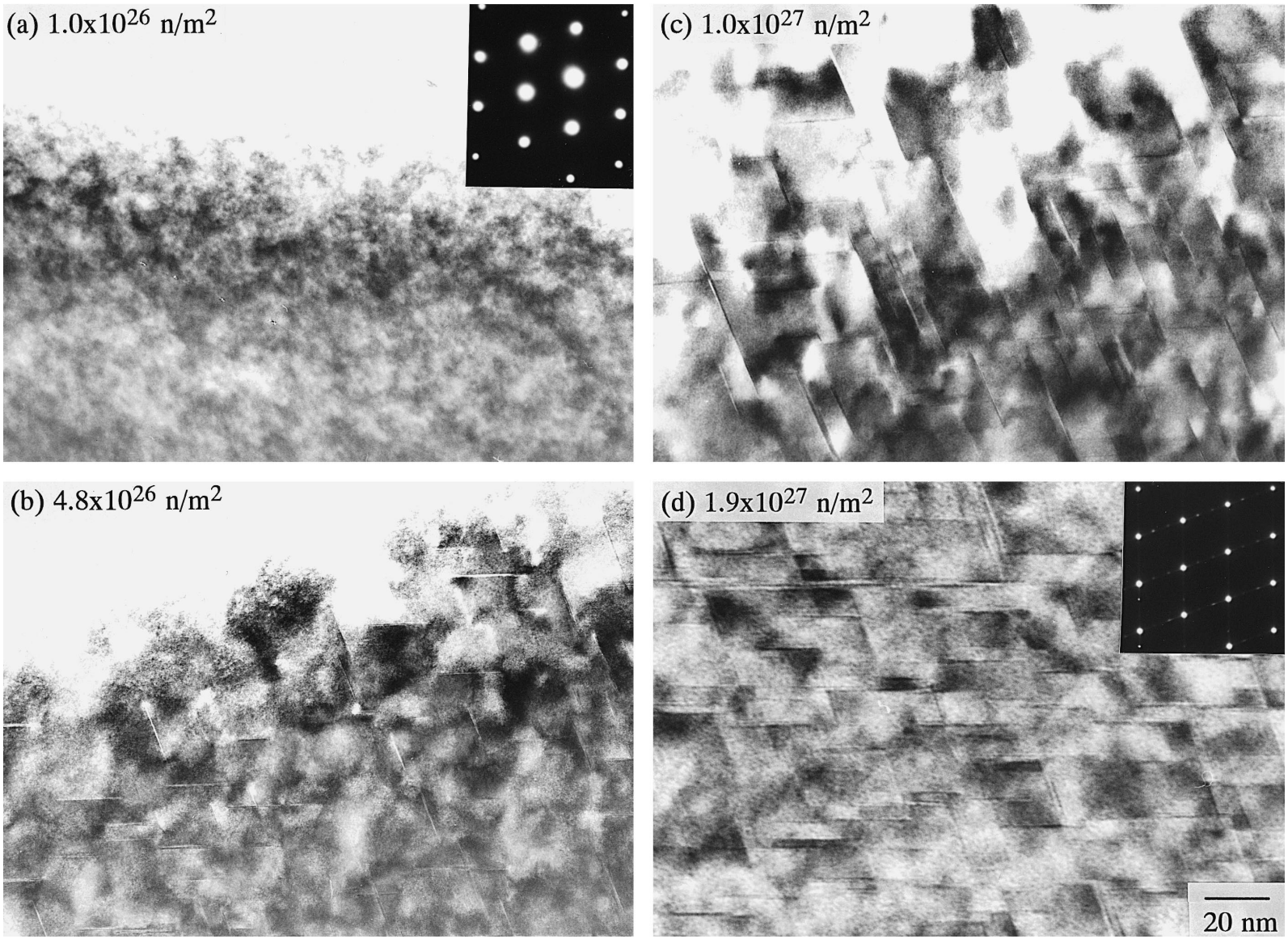

Fig. 5. Bright field electron micrographs of specimens irradiated to (a) 1.0×10^{26}, (b) 4.8×10^{26}, (c) 1.0×10^{27} and (d) 1.9×10^{27} n/m^2, taken along the [110] incident beam direction. Selected area diffraction patterns are also shown in (a) and (d).

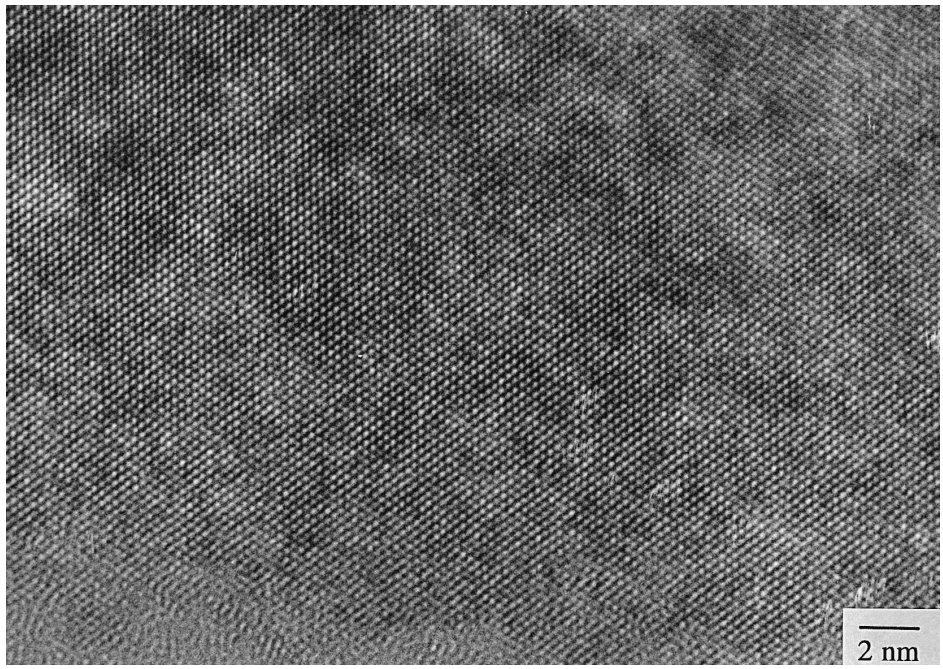

Fig. 6. High-resolution electron micrograph of the specimen irradiated to 1.0×10^{26} n/m^2, taken along the [110] incident beam direction.

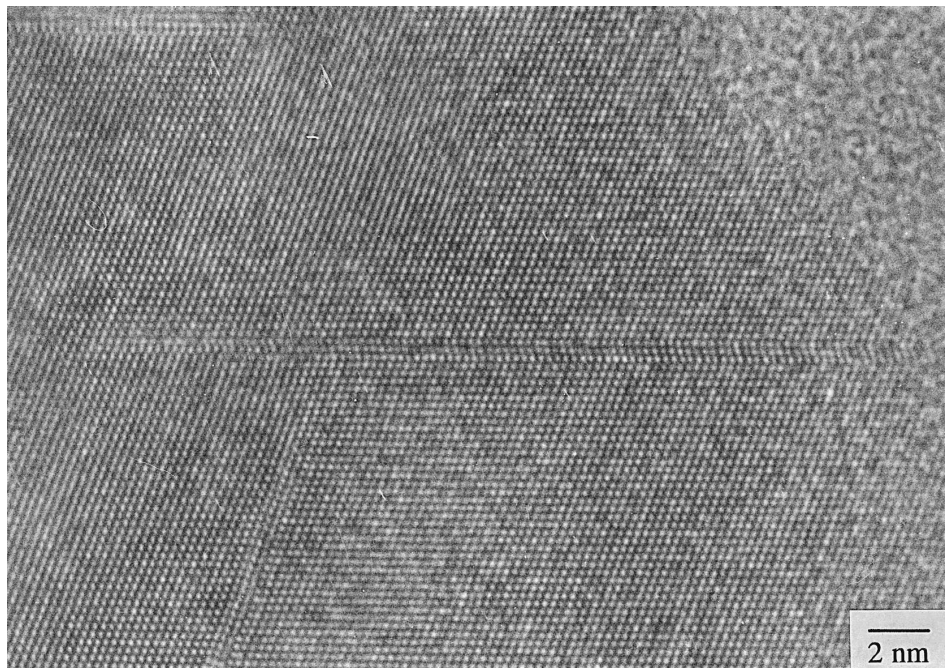

Fig. 7. High-resolution electron micrographs of the specimen irradiated to 1.0×10^{27} n/m^2, taken along the [110] incident beam direction.

smaller, about 10 nm, for the specimen irradiated to 4.8×10^{26} n/m^2. The spacing between each dislocation loop is about 10 to 20 nm, in good agreement with the crystallite size obtained from the X-ray diffraction measurements.

Based on the experimental results described above, we have concluded that the agglomerated defects such as interstitial dislocation loops nucleate at fluences of about 1×10^{26} n/m^2, and grow relatively large by 2×10^{26} n/m^2. Before formation of interstitial loops, the irradiation-induced defects retain a point defect character, such as single, di- or tri-point defects of interstitials and vacancies, and induce isotropic lattice expansion. In this stage, the linear expansion of the specimens corresponds very well with the growth of the lattice parameters and gives rise to slight broadening of X-ray diffraction peak profiles with only a small strain contribution. After the formation of small defect clusters such as loops, the effective crystallite size decreases relatively quickly due to its dependence on the density of clusters. The surviving vacancy defects remain as point-like structures, since the migration of vacancies appears limited below 1200°C from void swelling [12] and the formation of He bubbles [20]. As a result of interstitial loop formation, excess vacancy-type point defects in the crystal lead to homogeneous lattice contraction. Small interstitial clusters lead to lattice distortion associated with lattice strain. In this stage, the diffraction peaks show significant broadening due to both crystallite size and the strain effects, whereas most atoms constitute the regular crystal arrangement inside each of the crystallites. Parts of the crystalline lattice are deformed by the strain fields around the interstitial loops.

3.2. Effect of thermal annealing

The changes in lattice parameter and macroscopic length with increasing annealing temperature for the specimen irradiated to a fluence of 1.7×10^{27} n/m^2 are shown in Fig. 8 [14,15]. The holding time at each temperature was 1 h. This specimen shows significant XRD peak broadening after neutron irradiation (Fig. 2). Neither lattice parameter nor macroscopic length was influenced by annealing up to the irradiation temperature of around 400°C. The values of these two properties start to decrease above that temperature and continuously decrease up to around 1200°C. The rates of lattice parameter and macroscopic length decrease are almost the same. It is worth noting that the lattice parameter decreases to below the pre-irradiation value above 700°C. Above 1200°C, the lattice parameter increases and finally returns to the pre-irradiation value after annealing at 1800°C. On the other hand, the macroscopic length decreases continuously up to 1400°C. Almost identical recovery behavior for macroscopic length and lattice parameter was observed for the specimen irradiated to a fluence of 4.8×10^{26} n/m^2.

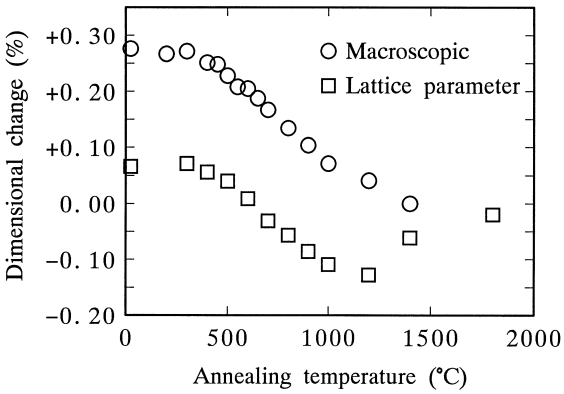

Fig. 8. Changes in lattice parameter and macroscopic length with increasing annealing temperature for the specimen irradiated to a fluence of 1.7×10^{27} n/m^2. Holding time at each temperature was 1 h.

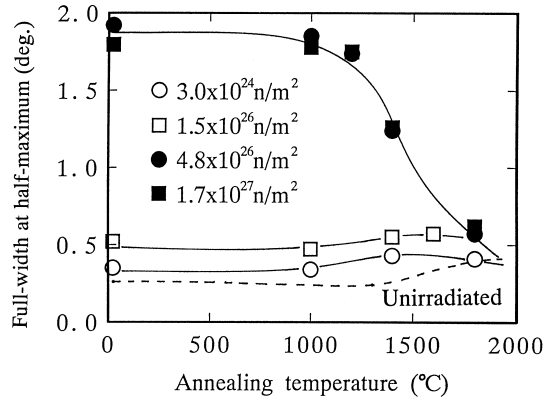

Fig. 9. Plot of the change in full-width at half-maximum of the (333)/(511) reflection as a function of annealing temperature for specimens irradiated to various fluences.

The changes in the FWHM of the (333)/(511) reflection as a function of annealing temperature are shown in

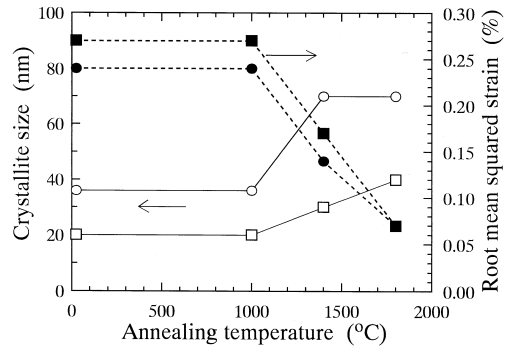

Fig. 10. A plot of crystallite size and the root mean squared strain against annealing temperature for specimens irradiated to 4.8×10^{26} (square mark) and 1.7×10^{27} n/m^2 (circle mark). Note the lack of change in the 1000°C as compared to the un-annealed specimen.

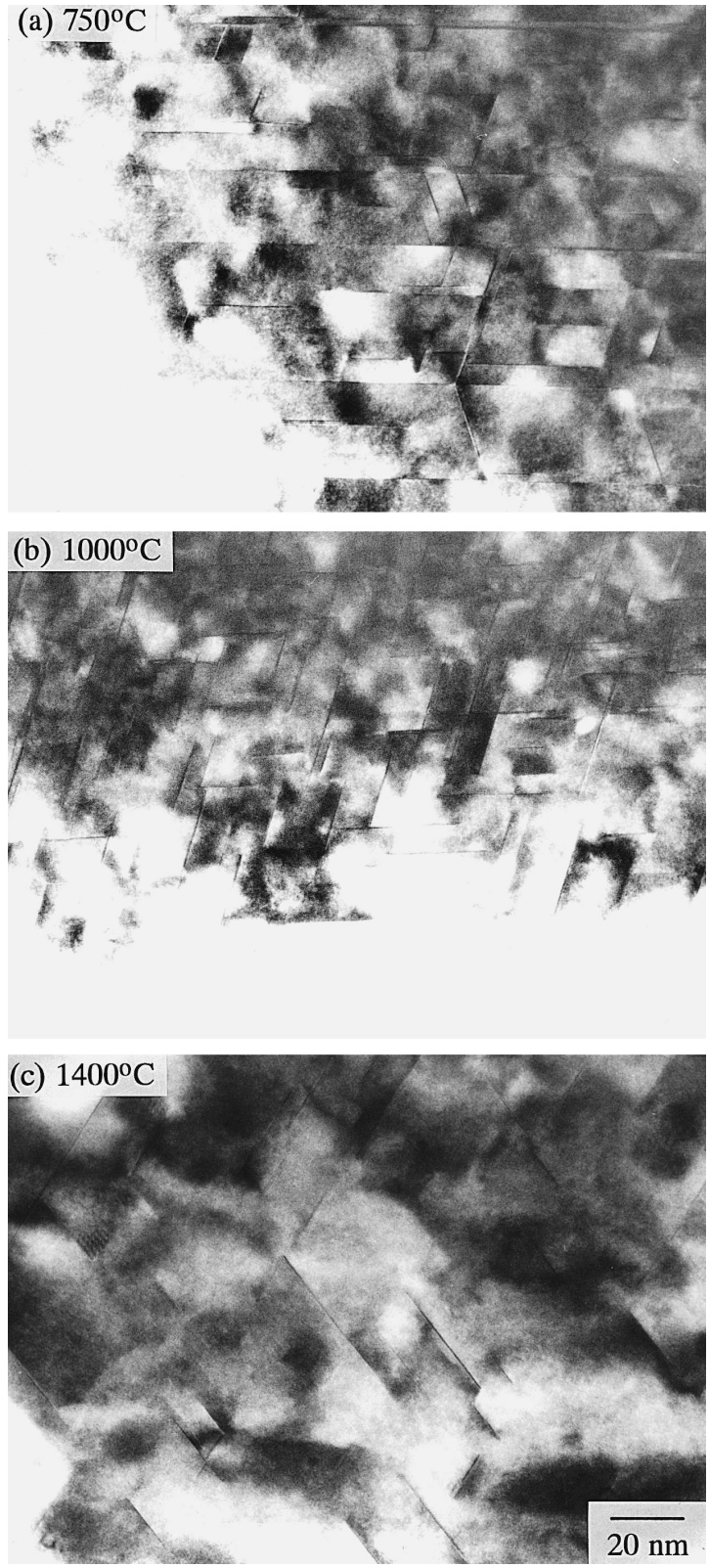

Fig. 11. Bright-field electron micrographs of the specimen irradiated to 1.0×10^{27} n/m^2 and annealed at (a) 750, (b) 1000 and (c) 1400°C for 1 h.

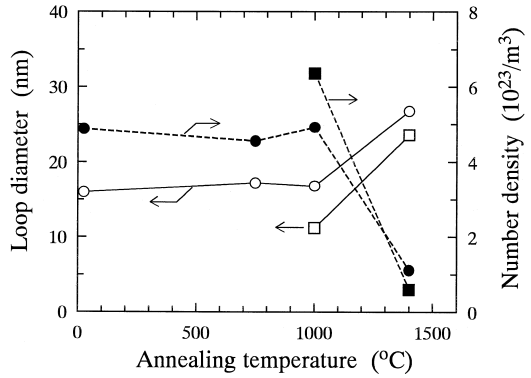

Fig. 12. Average diameter (unfilled symbols) and number density of interstitial loops (filled symbols) as a function of annealing temperature for specimens irradiated to 4.8×10^{26} (squares) and 1.0×10^{27} n/m^2 (circles).

Fig. 9 [14]. The peak broadening for the specimens irradiated to 1.5×10^{26} n/m^2 changes only slightly up to 1800°C, as is the case for the unirradiated specimen. The (333)/(511) FWHM for specimens irradiated to 4.8×10^{26} n/m^2 or higher remains at pre-annealing values up to 1000°C and decreases slightly after 1200°C annealing. Above 1200°C, these values decrease markedly and eventually reach the value of the lower fluence specimens.

In Fig. 10, the effect of temperature on crystallite size and rms strain for specimens irradiated to fluences of 4.8×10^{26} and 1.7×10^{27} n/m^2 is presented. The data taken at 1000°C were judged to be identical to those for the as-irradiated specimen because the FWHM of the specimen annealed at 1000°C showed a completely similar profile to that of the un-annealed specimen (Fig. 9). Note that both the rms strain and crystallite size are unchanged after annealing at 1000°C. Annealing at 1400°C and 1800°C progressively reduced the rms strain and increased the crystallite size.

A series of electron micrographs of the specimen irradiated to a fluence of 1.0×10^{27} n/m^2 after annealing at elevated temperatures is shown in Fig. 11. Up to a temperature of 1000°C, the size and density of interstitial loops do not change detectably, whereas the loop distribution coarsens noticeably after annealing at 1400°C. The formation of voids was not observed up to 1400°C.

Fig. 12 shows the average interstitial loop diameter and number density for specimens irradiated to fluences of 4.8×10^{26} and 1.0×10^{27} n/m^2 as a function of annealing temperature [17]. The average size increases and the number density decreases after 1400°C annealing in both specimens.

Based on the above results, the annealing process of heavily irradiated SiC is presumed to be as follows. Below the irradiation temperature, there is no change in defect concentration and structure. Between the irradiation temperature and around 1200°C, the macroscopic length and lattice parameter decrease concurrently and at the same rate as that shown in Fig. 8. Up to 1200°C, there are minimal changes in X-ray line broadening (Fig. 9). Marked changes in the size and number density of interstitial loops are found at 1400°C (Figs. 10–12). Therefore, we believe that interstitials start to migrate above the irradiation temperature and annihilate with vacancies, which cannot migrate below 1200°C. During this stage, therefore, reduction of point-like defects of interstitials and vacancies occur in the same number. As recombination proceeds, the number of residual vacancies becomes much greater than the number of residual interstitial point defects. This is because a large fraction of the interstitial atoms, which are created by neutron irradiation in equal number with vacancies, are condensed into interstitial loops during irradiation. This situation of excess vacancy-type point-defects leads to lattice contraction. Above 1200°C, the migration of vacancies occurs gradually; they will recombine with interstitials trapped at smaller interstitial loops. In this stage, the density of vacancy-type defects decreases, leading to lattice expansion and a reduction in small interstitial loops. The decrease in number density of smaller loops and the increase in the size of larger loops occurs concurrently above 1200°C by the net flow of vacancies from larger loops to smaller loops. In this way smaller loops eventually vanish. The decrease in number density of interstitial loops results in an increase in crystallite size and a decrease in lattice strain, and consequently the reduction of FWHM. Further precise study is required to determine the annealing mechanism of SiC irradiated to very high fluences.

4. Conclusion

Silicon carbide neutron-irradiated to fluences up to 1.9×10^{27} n/m^2 at 370–650°C was examined by X-ray diffractometry and electron microscopy. The results obtained are summarized as follows.

(1) A critical fluence for irradiation effects in SiC was revealed to be around 2×10^{26} n/m^2 at irradiation temperatures around 500°C. Up to this fluence, irradiation-induced interstitials and vacancies are preserved as point defects, whereas beyond this fluence interstitials agglomerate into dislocation loops on {111}.

(2) In accord with the change in defect structure, there are reductions in crystallite size and increases in the rms strain in specimens irradiated to more than the critical fluence. Even though the crystallite size decreases, good crystallinity is maintained and no signs of amorphization were observed. No voids were observed, even for the highest fluence specimen.

(3) From observations of recovery by thermal annealing of specimens irradiated to more than the critical fluence, it is expected that the irradiated specimens contain vacancies

and interstitials as well as interstitial loops. The number of vacancy defects is higher than the number of free interstitials.

(4) During annealing, interstitial atoms first migrate and combine with vacancies, and then vacancies start to migrate above 1200°C. The lattice parameter may drop below the pre-irradiation value during the annealing stage. Until 1400°C, formation of voids was not observed.

Acknowledgements

This work was partly supported by a Grant-in-Aid for Scientific Research from the Ministry of Education, Science, Sports and Culture, Japan. The specimens were kindly supplied by Power Reactor and Nuclear Fuel Development Corporation, Japan. A part of the experiment was carried out at the Irradiation Experiment Facilities, Institute of Materials Research, Tohoko University.

References

[1] G.R. Hopkins, R.J. Price, Nucl. Eng. Design/Fusion 2 (1985) 111.
[2] R.H. Jones, C.H. Henager Jr., G.W. Hollenberg, J. Nucl. Mater. 191–194 (1992) 75.
[3] L.L. Snead, S.J. Zinkle, D. Steiner, J. Nucl. Mater. 191–194 (1992) 560.
[4] P. Fenici, H.W. Scholz, J. Nucl. Mater. 212–215 (1994) 60.
[5] H.W. Scholz, M. Zucchetti, K. Casteleyn, C. Adelhelm, J. Nucl. Mater. 212–215 (1994) 655.
[6] L.L. Snead, R.H. Jones, A. Kohyama, P. Fenici, J. Nucl. Mater. 233–237 (1996) 26.
[7] S.D. Harrison, J.C. Corelli, J. Nucl. Mater. 122&123 (1984) 833.
[8] J.C. Correlli, J. Hoole, J. Lazzaro, C.W. Lee, J. Am. Ceram. Soc. 66 (1983) 529.
[9] R.J. Price, Nucl. Technol. 35 (1977) 320.
[10] C.H. Wu, J.P. Bonal, B. Kryger, J. Nucl. Mater. 208 (1994) 1.
[11] T. Suzuki, T. Yano, T. Mori, H. Miyazaki, T. Iseki, Fusion Technol. 27 (1995) 314.
[12] R.J. Price, J. Nucl. Mater. 48 (1973) 47.
[13] R.J. Price, J. Nucl. Mater. 33 (1969) 17.
[14] H. Miyazaki, T. Suzuki, T. Yano, T. Iseki, J. Nucl. Sci. Technol. 29 (1992) 656.
[15] T. Iseki, T. Yano, H. Miyazaki, J. Nucl. Mater. 191–194 (1992) 588.
[16] T. Yano, T. Iseki, Philos. Mag. A 62 (1990) 421.
[17] T. Yano, T. Suzuki, T. Maruyama, T. Iseki, J. Nucl. Mater. 155–157 (1988) 311.
[18] H.P. Klug, L.E. Alexander, X-ray Diffraction Procedures for Polycrystalline and Amorphous Materials, Wiley, New York, 1974.
[19] J.E. Palentine, J. Nucl. Mater. 92 (1980) 43.
[20] K. Sasaki, T. Yano, T. Maruyama, T. Iseki, J. Nucl. Mater. 179–181 (1991) 407.